excess energy in butynal, $H_3CC{\equiv}CCHO$, illustrates the transition from simple quantum beat decays to biexponential fluorescence decays as depicted in Figure 7. The fast decay component in part b originates from a large number of quantum beats, prepared in phase at the incidence of the laser pulse, but shortly after they interfere destructively. As some oscillations come back into phase at a later time, recurrence spikes appear superimposed on the slow decay component.[23] Investigation along this line, in particular in view of the level statistics and the dynamics in molecules, are in progress.

In our conclusion, we should reevaluate the resolving power of quantum beat spectroscopy. Lifetimes of 1–10 μs provide a resolution of 150–15 kHz, which in conventional spectroscopy may prove difficult to achieve, but can be readily obtained in quantum beat spectroscopy regardless of the laser bandwidth. From the experimental point of view, it is the total observation time that limits the resolution. However, the resolution may be improved even beyond the natural linewidth if the emission of the *ensemble* of the excited molecules is biased in favor of the long-lived species in the data analysis.[24] The gain in resolution, as shown in the example in Figure 8, is in accordance with Heisenberg's uncertainty principle because the natural linewidth is valid only for a nonselected ensemble of excited molecules decaying by spontaneous emission.

Clearly, quantum beat spectroscopy on the nano- and microsecond time scales is used advantageously whenever transitions should be resolved within the Doppler profile of a conventional spectrum. On the other hand, high temporal resolution, i.e., short pulse duration and short sampling intervals, allows us to detect high frequencies. Quantum beat frequencies exceeding the Doppler width can be observed with pico- or femtosecond resolution, but the corresponding energy differences are resolvable with less experimental effort by conventional spectroscopic methods. Thus, for high resolution in the energy domain, be slow, wait long enough, and use quantum beats...!

We acknowledge continuous support of our laser spectroscopic work by the Swiss National Science Foundation and the University of Zürich.

(24) Dodd, J. N.; Series, G. W. In *Progress in Atomic Spectroscopy*; Hanle, W., Kleinpoppen, H., Eds.; Plenum: New York, 1978; Part A, Chapter 14.

Orbital Stereochemistry: Discovering the Symmetries of Collision Processes

STEPHEN R. LEONE

Joint Institute for Laboratory Astrophysics, National Institute of Standards and Technology and University of Colorado, and Department of Chemistry and Biochemistry, University of Colorado, Boulder, Colorado 80309

Received September 24, 1991 (Revised Manuscript Received November 26, 1991)

Introduction

One of the most exciting recent aspects of laser chemistry is the ability to prepare highly aligned, or directional, reagents using the polarization of lasers.[1-5] It is now possible to investigate chemical processes with directional control in a variety of new measurements. The results provide a means of visualizing the important symmetries of the chemical process with unprecedented detail. Many mechanistic interpretations of chemical transformations are built upon compelling pictures of orbital directionality, electron overlap and transfer, and symmetry arguments.[6] Chemists can exploit the methods of directional control to verify these pictures and to broaden our understanding of chemical stereospecificity.

Consider, for example, a simple case of a p orbital, which can be prepared with a laser from a ground s state and aligned along the direction of polarization of the light. The p orbital may be aligned parallel or perpendicular to an oncoming collision partner by using well-defined crossed beams of reagents and by arranging the polarization of the excited light in the desired direction with respect to the relative velocity of approach (Figure 1). If a hypothetical chemical reaction requires the orbital to approach preferentially in the perpendicular direction in order to produce a favorable electron overlap, then a larger rate coefficient might be observed for the initial perpendicular orbital configuration than for the parallel preparation of the p state. With an appropriate mathematical formalism, it can be shown that the rate coefficient will increase and decrease smoothly with the form of a cos (2β) function, repeating every 180° when the direction of the p orbital is rotated. Here β is the angle between the direction that the orbital lobes make with the relative velocity vector, as shown in Figure 1. The result gives a direct determination of the relevant orbital stereochemistry that is required for the reaction, i.e., an orbital alignment effect.

Stephen R. Leone was born in New York City in 1948. He is presently Chairman of the Joint Institute for Laboratory Astrophysics and a Fellow of the National Institute of Standards and Technology (formerly the National Bureau of Standards) in the Quantum Physics Division. He is concurrently a Professor Adjoint in the Department of Chemistry and Biochemistry at the University of Colorado. He received his B.A. degree in chemistry from Northwestern University in 1970 and his Ph.D. degree under the direction of C. Bradley Moore at the University of California, Berkeley, in 1974. From 1974 to 1976 he was a faculty member at the University of Southern California, before assuming his position in Boulder, CO.

(1) Bernstein, R. B.; Herschbach, D. R.; Levine, R. D. *J. Phys. Chem.* **1987**, *91*, 5365–5377.
(2) Simons, J. P. *J. Phys. Chem.* **1987**, *91*, 5378–5387.
(3) Houston, P. L. *J. Phys. Chem.* **1987**, *91*, 5388–5397.
(4) Whitehead, J. C. *Selectivity in Chemical Reactions*; Kluwer Academic Publishers: Dordrecht, The Netherlands, 1988.
(5) Stolte, S., Parker, D. H., Eds. Richard Bernstein Memorial Issue. *J. Phys. Chem.* **1991**, *95*, 7961–8421.
(6) Woodward, R. B.; Hoffmann, R. *The Conservation of Orbital Symmetry*; Verlag Chemie, Academic Press: Weinheim, Germany, 1971.

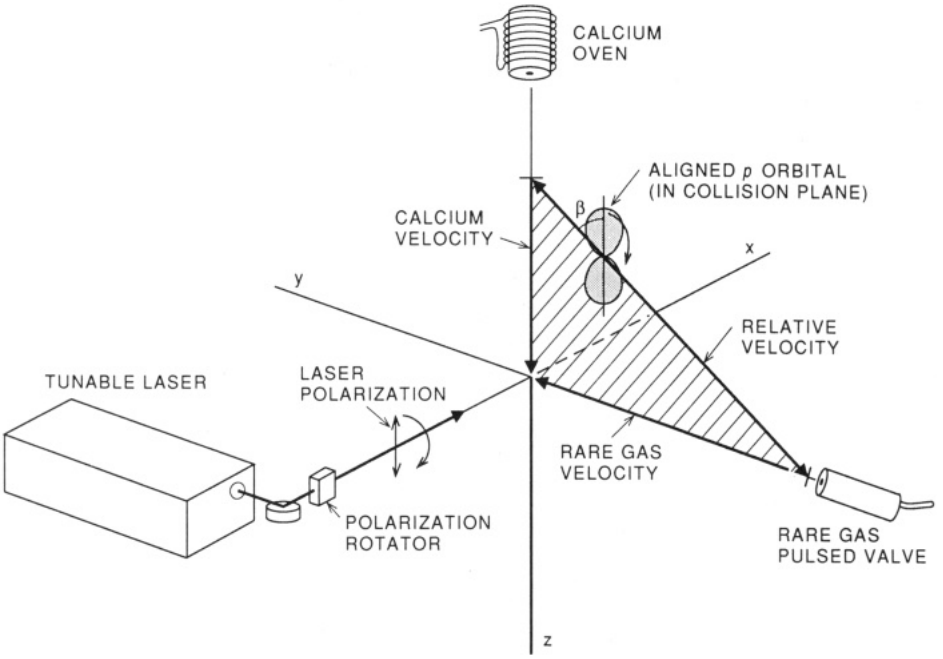

Figure 1. Schematic representation of the experimental arrangement for orbital alignment studies, showing the laser polarization and p-orbital preparation with respect to the relative velocity in the collision.

While it is possible to select the directionality of molecules with lasers or with modulated fields, this Account considers primarily studies of laser-aligned atomic orbitals. A wide variety of chemical reactions have now been studied to determine alignment preferences, by varying either molecular or atomic orbital directions.[1,2] However, simpler collisional energy transfer experiments are a remarkably useful starting point to understand the chemistry of alignment preferences. Such experiments investigate changes of atomic states induced by collisions, for example, a change from a d state to an f state, or a singlet p state (^{1}P) to a triplet p state (^{3}P). These processes, called near resonant electronic energy transfer, come about by crossings between molecular potential energy curves during the collision. Results of this type of experiment show a richness of alignment detail which can be understood with a few simple principles and quantitative theoretical calculations.

This Account considers the effects of orbital stereochemistry for p, d, and f states of atomic Ca atoms in collisions with nonreactive rare gas atoms. One, two, or three lasers of different colors are used to prepare the p, d, or f atomic orbitals, respectively, with different initial geometries and directions of the orbital wave functions. In some circumstances the results allow a remarkable visualization of the effective shapes of the initially prepared orbitals as they are sampled in the collision process. In more ambitious experiments, both the initial orbital alignment can be set and the alignment of the final state detected. In addition, the scattering into specific angles following collisions of aligned reagents can now be probed. This allows, with some measure of interpretation, a full specification of the alignment effects involved in the energy-transfer event.

Mechanics of the Alignment Process

We start with a picture of several molecular van der Waals potential energy curves, shown in Figure 2.

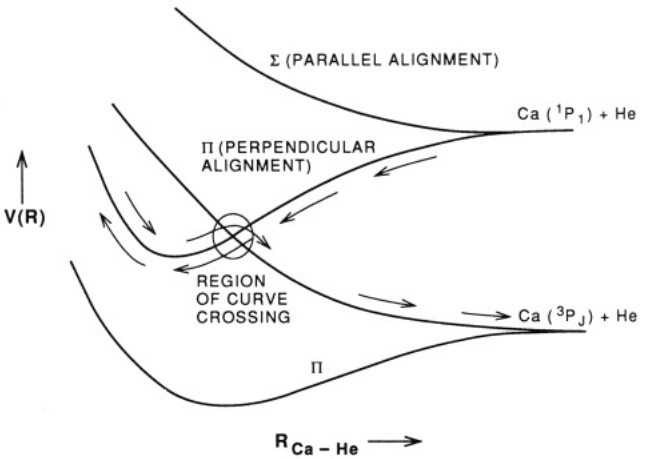

Figure 2. Hypothetical van der Waals potential energy curves for two near-resonant electronic states of Ca colliding with He. A typical curve-crossing path is shown by the arrows. The Π molecular state, or perpendicular orbital alignment, would preferentially lead to the energy transfer from ^{1}P$_1$ to ^{3}P$_J$.

There are two near-resonant 5p electronic states, Ca 4s5p ^{1}P$_1$ and Ca 4s5p ^{3}P$_J$, and we will study the rate of energy transfer between these two states induced by collisions with He. Here J refers to the group of three closely spaced fine structure levels J = 0, 1, and 2. If the Ca ^{1}P$_1$ state is initially excited with its p-orbital wave function parallel to, or pointing toward, the approach direction of the He, the electrons of the orbital and the He atom overlap, causing primarily a repulsive interaction, shown by the Σ molecular state. If the orbital is initially prepared perpendicular to the approach of He, the positive ion core of the excited Ca can attract the electrons on the He, leading to the initially attractive curve labeled Π; when the atoms get very close together, repulsion again begins to dominate. Both the Ca ^{1}P$_1$ and Ca ^{3}P$_J$ states have very similar molecular interaction potentials, and thus the Ca ^{3}P$_J$ + He also has an attractive Π molecular state and a repulsive Σ molecular state, as shown in the figure.

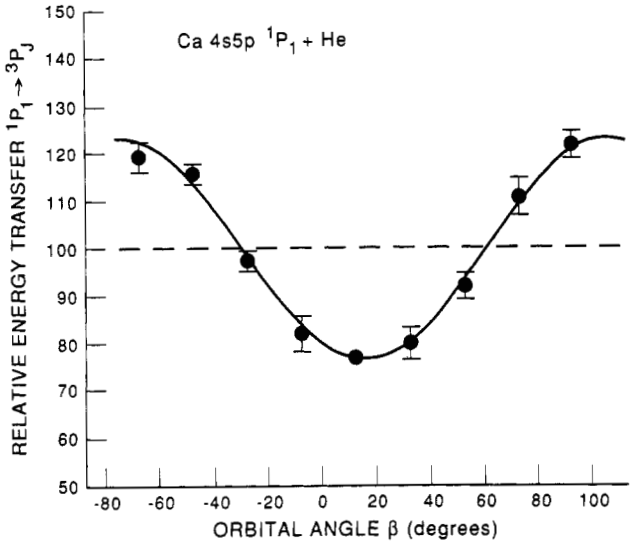

Figure 3. Alignment data (relative energy transfer versus orbital angle) for the transfer from Ca $^1P_1$ to ^3P_J induced by collision with He.

Since the energy difference between the Ca $^1P_1$ and ^3P_J states is small, the Π molecular state from the $^1P_1$ might cross with the repulsive Σ state arising from the ^3P_J states. Thus the Ca $^1P_1$ Π state can lead preferentially to the formation of the ^3P_J state.

Herein lies a fundamental mechanistic explanation for why the initial perpendicular orbital alignment might have a faster rate than the parallel configuration for Ca 4s5p $^1P_1$ collisions with He. With laser preparation of the states in a crossed-beam arrangement, such an effect is detected by fluorescence from the product state as a function of orbital alignment (Figure 3): the perpendicular orbital alignment of the $^1P_1$ state is found to be 1.6 times more efficient at populating the ^3P_J state than the parallel alignment.[7,8] The shape of the signal which describes the alignment effect in Figure 3 is a cos (2β) function, as noted above, where the angle β corresponds to the angle the orbital lobe makes with respect to the relative velocity, or direction of approach of the collision partners (Figure 1). The observed maxima in the signal are located at approximately $\beta = \pm 90°$, indicating that the perpendicular orbital alignment has the larger rate coefficient for the energy transfer. Not all of the observed effects favor the perpendicular orbital alignment, depending on the specific placements of the potential energy curves.

Not all collisions occur directly head-on, but rather most of the collisions are near misses. Figure 4 shows an example of a straight-line trajectory for such a near-miss type of collision. The orbital is aligned initially in the parallel configuration. In the absence of forces the orbital tends to remain aligned along its initial path. However, there are electrostatic forces which act on the orbital causing it to try to preserve its alignment with respect to the internuclear axis, an effect which is called "locking" to the molecular frame.[9,10] In the case of a p orbital, the energy splitting between the Σ and Π states (Figure 2) causes a torque on the orbital. The finite velocity of the collision partners limits the effect of this torque. Long interaction times (low velocities) tend to preserve the initial alignment with respect to the internuclear axis (locking), while for short interaction times (high velocities) the orbital tends to remain unaffected by the torque (remains space-fixed). At typical velocities in these experiments, calculations show that the locking is only partial; visually the orbital would appear to precess throughout the trajectory (Figure 4).[11,12] This partial locking causes the magnitude of the observed alignment effect to be diminished, compared to the case if all collisions could be prepared exactly head-on. In addition, the degree of "near miss" varies for each collision, thus potentially sampling a wide range of alignment angles. In real systems, there can also be multiple potential curves and crossings. Each of these effects can reduce the observed alignment. Simple estimates suggest that if the intrinsic alignment effect has a 100:1 preference, it can easily be reduced to an effect of only 2:1 in the actual observation.

Formally, the p orbital is prepared with respect to the laser polarization in a pure p_z state ($m = 0$ angular momentum sublevel), or the $Y_{1,0}$ spherical harmonic. With respect to the oncoming collision partner, this orbital can then be aligned initially parallel or perpendicular. For simplicity, we will describe the collision process in the collision frame, where the relative velocity of approach serves as the z-axis and the orbital makes an angle β with respect to this axis. Thus, the parallel orbital alignment is the pure p_z orbital, and the perpendicular orbital alignment is the p_x orbital. Recall that the p_x and p_y orbitals are formed out of superpositions of the pure angular momentum states, i.e., the $m = 1$, $Y_{1,1}$ (p_+) and $m = -1$, $Y_{1,-1}$ (p_-) wave functions.

A typical, near-miss type of collision samples not only the $m = 0$ component of the wave function but also the $m = \pm 1$ components. The $m = 0$ component is related to the parallel alignment, or the molecular Σ state in Figure 2, and the $m = \pm 1$ components are related to the perpendicular orbital alignment, or the molecular Π state in Figure 2. The fractions of $m = 0$ and $m = \pm 1$ that contribute to the observed rate of energy transfer depend on the direction of the initial asymptotic orbital preparation, which the experimentalist can control, as well as the degree of orbital locking and following. The observed shape of the alignment signal can be worked out mathematically; it depends on the mathematical form of the orbital *wave function* (not the electron density) as it is rotated with respect to the relative velocity.[8] For a p state the resulting signal shape is the cos (2β) function noted above. A measurement of the alignment effect gives the individual m-sublevel contributions ($m = 0$ vs $m = \pm 1$) to the total rate constant, or cross section, for the energy transfer.

More Complex Orbitals

While the notion of orbital directionality is a relatively straightforward concept to visualize for p states, for higher d and f states there are more elaborate symmetries and a greater variety of wave functions possible.

(7) Hale, M. O.; Hertel, I. V.; Leone, S. R. *Phys. Rev. Lett.* **1984**, *24*, 2296–2299.
(8) Bussert, W.; Neuschäfer, D.; Leone, S. R. *J. Phys. Chem.* **1987**, *87*, 3833–3842.
(9) Hertel, I. V.; Schmidt, H.; Bähring, A.; Meyer, E. *Rep. Prog. Phys.* **1985**, *48*, 375–414.
(10) Campbell, E. E. B.; Schmidt, H.; Hertel, I. V. *Adv. Chem. Phys.* **1988**, *72*, 37–114.
(11) Kovalenko, L. J.; Leone, S. R.; Delos, J. B. *J. Chem. Phys.* **1989**, *91*, 6948–6960.
(12) Schatz, G. C.; Kovalenko, L. J.; Leone, S. R. *J. Chem. Phys.* **1989**, *91*, 6961–6972.

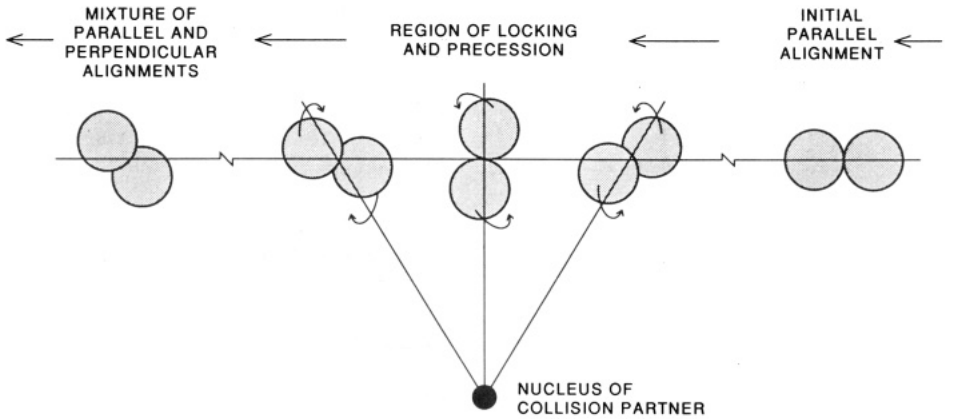

Figure 4. A typical near-miss trajectory of a p orbital showing the tendency for orbital locking and precession due to electrostatic forces.

Figure 5 shows two different wave functions each for a d and an f state; the d and f states can be prepared by excitation with two[13] and three[14] polarized laser pulses, respectively. The two different wave functions can be selected by using collinear laser beams either with parallel polarizations (Figure 5a,c) or with one laser polarization perpendicular to the others (Figure 5b,d). The prepared wave functions are mathematically described by spherical harmonics corresponding to $Y_{2,0}$ and the superposition state $(Y_{2,-1} - Y_{2,1})/2^{1/2}$ for the d states and to $Y_{3,0}$ and the superposition state $(Y_{3,-1} - Y_{3,1})/2^{1/2}$ for the f states.

Note that the $Y_{2,0}$ is a d_{z^2} orbital and the $(Y_{2,-1} - Y_{2,1})/2^{1/2}$ wave function is a d_{xz} orbital. As can been seen from the figure, the $Y_{2,0}$ and $Y_{3,0}$ states have two large lobes with one or two tori around the waist for d or f states, respectively, while the $(Y_{2,-1} - Y_{2,1})/2^{1/2}$ and $(Y_{3,-1} - Y_{3,1})/2^{1/2}$ look like a 4-fold propeller (d state) and a six-bladed, unsymmetrical cloverleaf (f state). The latter orbital may be unfamiliar to readers, but it is just a result of a different superposition of the fundamental *m*-sublevel wave functions. If the laser beams are propagated in more general directions, for example, with three mutually perpendicular polarizations, other orbitals can be prepared, such as the more familiar and chemically useful f_{xyz} orbital, which has eight lobes and is described by the wave function $(Y_{3,-2} - Y_{3,2})/2^{1/2}$.

When alignment experiments are carried out with the d or f states, complicated signals result, which reveal the higher-fold symmetry of the atomic wave functions. For example, with d states, one expects to observe both 2-fold and 4-fold cosine function oscillations $[a_0 + a_2 \cos(2\beta) + a_4 \cos(4\beta)]$,[13] and f states exhibit the sum of 2-fold, 4-fold, and 6-fold oscillations $[a_0 + a_2 \cos(2\beta) + a_4 \cos(4\beta) + a_6 \cos(6\beta)]$.[14,15]

A very clear example may be seen in the signals for the d-state energy transfer shown in Figure 6, for the process $Ca(4p^2\,{}^1D_2) + Ne \rightarrow Ca(3d4f\,{}^1F_3) + Ne$. Emission from the $^1F_3$ final state is detected as a function of the initial orbital alignment angle β, set by the laser polarizations, with respect to the relative velocity in the collision (see Figure 5). When the two lasers are polarized perpendicular to each other (the signal in Figure 6b corresponding to the wave function

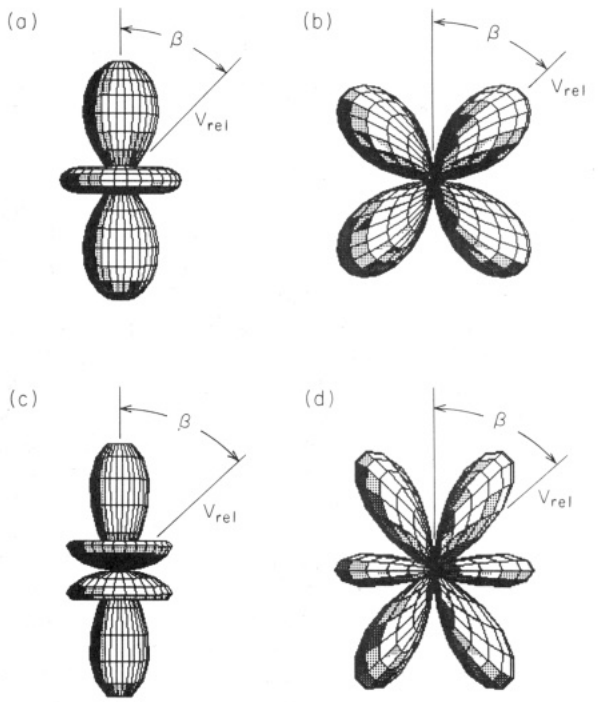

Figure 5. Wave functions for d and f orbitals prepared by two and three lasers, respectively. (a) $Y_{2,0}$ spherical harmonic (d_{z^2}) prepared by two parallel polarized lasers. (b) $(Y_{2,-1} - Y_{2,1})/2^{1/2}$ spherical harmonic (d_{xz}) prepared by two perpendicular polarized lasers. (c) $Y_{3,0}$ spherical harmonic (f state) prepared by three parallel polarized lasers. (d) $(Y_{3,-1} - Y_{3,1})/2^{1/2}$ spherical harmonic (f state) prepared by two lasers with parallel polarizations and one laser with polarization perpendicular to the other two.

in Figure 5b), the resulting signal variation is a very regular 4-fold cos (4β), repeating every 90°. The 4-fold shape of the wave function is mapped directly into the variation of the signal. When both lasers are parallel polarized, the alignment effect shows a strong 2-fold component with a weaker 4-fold component superimposed on top of it (the signal in Figure 6a corresponding to the wave function in Figure 5a). Once again the energy transfer rate is largest when the collision occurs between the lobes and torus of the wave function.

The dramatic change in signal shape between the two different orbital wave functions tells us that the shape of the wave function is definitely important in the collision. The signal variation in Figure 6a suggests that the effect is sensitive first of all of the two large lobes of the orbital, which gives rise to the 2-fold variation, and secondly to vestiges of the torus, which might cause

(13) Robinson, R. L.; Kovalenko, L. J.; Smith, C. J.; Leone, S. R. *J. Chem. Phys.* **1990**, *92*, 5260–5269.
(14) Driessen, J. P. J.; Smith, C. J.; Leone, S. R. *Phys. Rev. A* **1991**, *44*, R1431–R1434.
(15) Driessen, J. P. J.; Smith, C. J.; Leone, S. R. *J. Phys. Chem.* **1991**, *95*, 8163–8169.

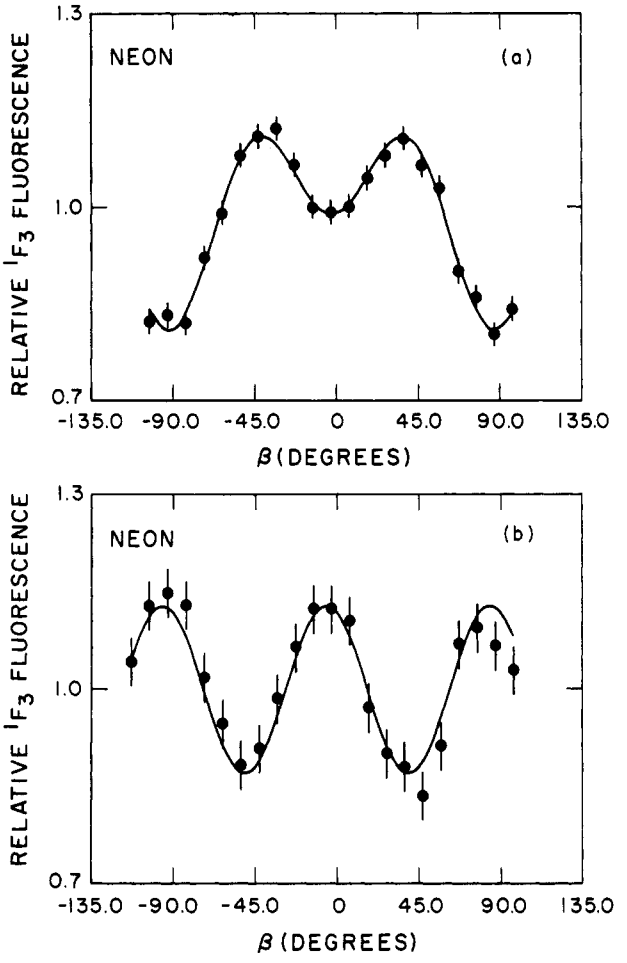

Figure 6. Alignment data versus orbital angle for (a) the d_{z^2} orbital and (b) the d_{xz} orbital. The latter shows clearly the 4-fold symmetry of the orbital wave function.

a 4-fold variation to be superimposed on top of the 2-fold signal. Since this is not a rigorously correct picture, in the next section we consider a more exact interpretation of the alignment effects carried out with these more complex orbitals.

Visualization of Orbital Shapes in Collisions

Since the alignment effects can become quite complicated, for example with f states including $a_0 + a_2 \cos(2\beta) + a_4 \cos(4\beta) + a_6 \cos(6\beta)$ terms, it becomes useful to display the signal variation in a way that is more readily visualized. Figure 7 shows one example for the collisions of $Ca(4s4f\,^1F_3)$ + Ar, which transfers the excitation to the $Ca(4p^2\,^1S_0)$ state. Rather than plotting the data of energy transfer rate versus angle β on a linear plot,[15] the data are displayed in a polar plot.[16] Thus the rate of energy transfer is plotted radially outward from the center, and the angle β (cf. Figure 5c,d) is plotted around in a circle. The relative velocity, which determines the collision direction, is shown by the straight lines through the data in Figure 7. It can be seen that these two polar plots look remarkably like the shapes of the two orbitals displayed in parts c and d of Figure 5, after rotating the orbitals so that vertical lines through the orbital wave functions in Figure 5 lie along the relative velocities in the respective polar plots. For example, in Figure 7a, one sees the two large lobes which mimic the wave function in Figure 5c and the two side bumps reminiscent of the tori. In Figure 7b, the six points of the wave function in Figure 5d are readily apparent. The results give remarkably clear evidence that subtle details of the orbital shapes are retained in the collisional energy transfer event.

However, one does not expect that the shapes of the wave functions should be reproduced so precisely in general. In fact, many other alignment effects that have been studied for the $^1F_3$ state and other rare gases do not look as much like the wave functions displayed in Figure 5.[15,16] What is the reason, then, that even the side lobes of the tori appear to be reproduced in Figure 7a? The answer is found when the alignment signals are decomposed into their component parts for the pure m-sublevel wave functions.

As pointed out previously, the wave function for an f state is described in the laser preparation frame by spherical harmonics, such as $Y_{3,0}$ or the superposition state $(Y_{3,-1} - Y_{3,1})/2^{1/2}$. In the collision frame, however, there are $m = 0$, $m = \pm 1$, $m = \pm 2$, and $m = \pm 3$ component wave functions which are sampled. These give rise to a number of molecular states which can lead to curve crossings that access the near-resonant state. These molecular states are Σ, Π, Δ, and Φ, respectively. Consider a specific example. Initially, the laser prepares a state, such as the $Y_{3,0}$ state. However, in the collision frame, this state corresponds to a mixture of $m = 0, \pm 1, \pm 2$, and ± 3 spherical harmonics. The corresponding rate constants or cross sections are related to this mixture with different weighting factors for each m-sublevel depending on which molecular curves are responsible for the energy transfer. Figure 8 shows what the polar plot signals would look like if each m-sublevel contributed equally to the alignment. Since there are plus and minus components for all but $m = 0$, the $m = \pm 1, \pm 2$, and ± 3 contributions are summed in the figure. As can be seen, when these contributions are added together with a unity weighting factor for each of the m components, the signal in the polar plot has no variation and is just a circle. There would be no observed alignment effect.

Since an alignment effect is observed for collisions of the Ca $^1F_3$ state with Ar, the relative contributions of the $m = 0, \pm 1, \pm 2$, and ± 3 components must not be equal. In fact they can be obtained from the measurements and are 1.94, 1.31, 0.69, and 0.53, for $m = 0$, $m = \pm 1$, $m = \pm 2$, and $m = \pm 3$, respectively.[15] These proportions are the m-sublevel resolved rate constants or cross sections. The rate constant for $m = 0$ is largest because the final state is a $^1S_0$ state, which has only the $m = 0$ state possible, and the $m = 0$ molecular curves in the initial and final states are preferentially coupled by motion along the internuclear axis. Using these weighting factors for the m-sublevel contributions, we obtain the polar plots of Figure 9, where Figure 9a displays the result for the $Y_{3,0}$ initial wave function and Figure 9b displays the result for the initial wave function $(Y_{3,-1} - Y_{3,1})/2^{1/2}$.

It can now be seen that the main lobes of Figure 9a are produced largely by the $m = 0$ component, or the molecular Σ state, while the two tori are due largely to the $m = \pm 3$ components, or the molecular Φ state. It should be noted that the intrinsic magnitudes of the $m = 0, \pm 1, \pm 2$, and ± 3 sublevel contributions are identical

(16) Driessen, J. P. J.; Leone, S. R. *J. Phys. Chem.*, to be published.

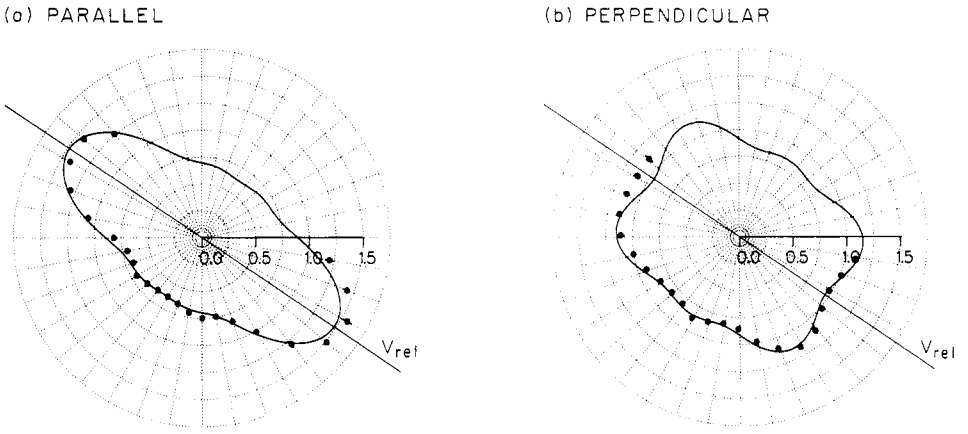

Figure 7. Alignment data for an f state in a polar type plot, with the relative rate (● = data) plotted radially outward and the angle β plotted around the circle. The relative velocity is shown as the straight line in each case and the best fit to the data by the curved line through the points. In part a, the $Y_{3,0}$ spherical harmonic is the initial state. In part b, the $(Y_{3,-1} - Y_{3,1})/2^{1/2}$ spherical harmonic is the initial state.

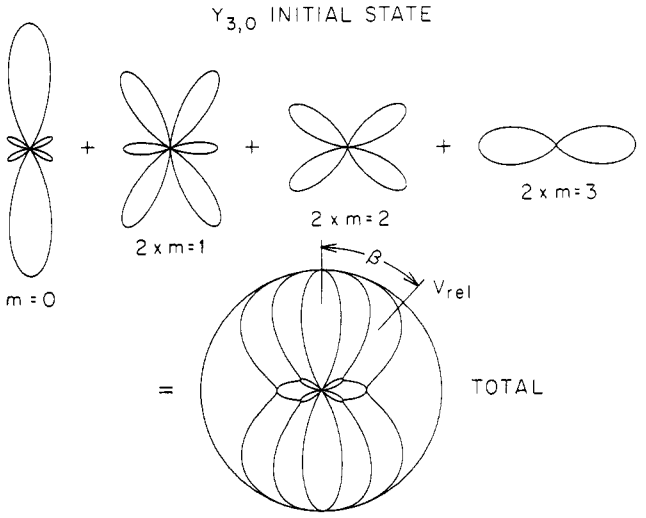

Figure 8. Deconvolution of the polar plot into the m-sublevel contributions with each m-sublevel contributing an equal weight.

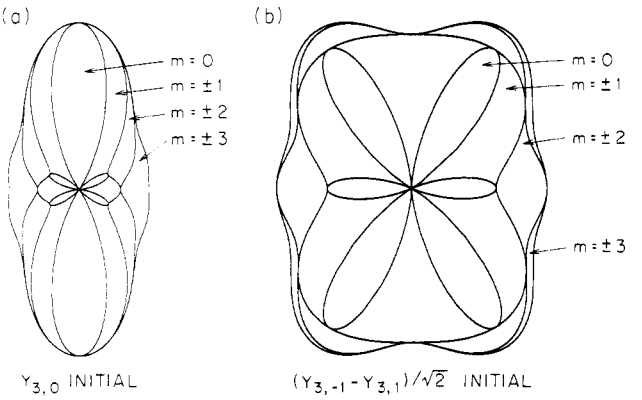

Figure 9. Deconvolution of the polar plot data in Figure 7 with the measured weighting factors for each m-sublevel contribution. In part a, the $Y_{3,0}$ spherical harmonic is the initial state. In part b, the $(Y_{3,-1} - Y_{3,1})/2^{1/2}$ spherical harmonic is the initial state.

for the initial $(Y_{3,-1} - Y_{3,1})/2^{1/2}$ state as well as the $Y_{3,0}$ state. It does not matter which wave function is initially prepared; the same relative rates are obtained. However, the shapes of the deconvolutions in parts a and b of Figure 9 are totally different. This reflects the fact that the $Y_{3,0}$ initial state is being tested in the collision in one case, the $(Y_{3,-1} - Y_{3,1})/2^{1/2}$ in the other. Because the rate constant or cross section for the $m = 0$ component of the wave function is the largest, it dominates the process. Mathematically, the $m = 0$ component always resembles the initial wave function, $Y_{3,0}$ or $(Y_{3,-1} - Y_{3,1})/2^{1/2}$ of part c and d of Figure 5, accounting for the observed shapes in Figure 9.

The Future of Alignment Studies

Orbital alignment studies presented above have revealed elegant details about the effective shapes of orbital wave functions in collisions. There are already many examples where alignment effects have been observed in chemical reactions, and the list is growing rapidly.[1,2,5] In our own laboratory, current work has addressed the question of alignment of the final state, after collision of an orbital that has been initially aligned. Intriguing preliminary results suggest that the orbitals frequently change directions after the state-changing collision. New experiments in other laboratories exploit the ability to align reagents to test the specific geometries that are favorable for reaction, such as in the adsorption and catalytic reactions of molecules on surfaces.

I enthusiastically acknowledge the exceptional talents and accomplishments of my students and postdoctorals who inspired this Account: Michael Hale, Dieter Neuschäfer, Wolfgang Bussert, Laurie Kovalenko, Ruth Robinson, Christopher Smith, and in particular Jan Driessen, who formulated the visualization polar plots shown here. There have been many successful collaborations with Ingolf Hertel, Eleanor Campbell, John Delos, George Schatz, Millard Alexander, and Brigitte Pouilly, which greatly prospered this research. The National Science Foundation is gratefully acknowledged for support of this work.